INVITED FEATURE PAPER

Thermophysical properties of SnO_2-based transparent conductive films: Effect of dopant species and structure compared with In_2O_3-, ZnO-, and TiO_2-based films

Nobuto Oka[a),c)] and Saori Yamada
Graduate School of Science and Engineering, Aoyama Gakuin University, Chuo, Sagamihara 252-5258, Japan
Takashi Yagi and Naoyuki Taketoshi
National Metrology Institute of Japan, National Institute of Advanced Industrial Science and Technology (AIST), Tsukuba, Ibaraki 305-8563, Japan
Junjun Jia and Yuzo Shigesato[b)]
Graduate School of Science and Engineering, Aoyama Gakuin University, Chuo, Sagamihara 252-5258, Japan

(Received 1 April 2014; accepted 11 July 2014)

We investigate the effect of dopant species and structure on the thermal conductivity of Sb-doped SnO_2 (ATO) and Ta-doped SnO_2 (TTO) films and compare the results with those of In_2O_3-, ZnO-, and TiO_2-based transparent conductive films. The thermal conductivities (λ) of polycrystalline ATO and TTO films are 4.4–4.9 and 4.7 W m^{-1} K^{-1}, respectively. The thermal conductivities via phonons (λ_{ph}) are almost identical for both dopant species (Sb and Ta): 4.3 and 4.5 W m^{-1} K^{-1} for Sb and Ta, respectively, on average. These results for λ_{ph} are larger than that for Sn-doped In_2O_3 films (3.8 W m^{-1} K^{-1}) and considerably larger than that for amorphous ATO films (1.0 W m^{-1} K^{-1}). These facts lead us to conclude that the base-material species (SnO_2 or In_2O_3) and structure (polycrystalline or amorphous) affect the thermophysical properties of ATO and TTO much more than the dopant species.

I. INTRODUCTION

SnO_2-based transparent conductive oxide (TCO) films, such as Sb-doped SnO_2 (ATO),[1–7] are the most chemically stable among TCO materials—an important prerequisite for several applications, such as solar cells. However, as Sb is undesirable for industrial applications because of its toxicity, it is important to find alternative doping materials. Among the possible alternative candidates, Ta shows promise, as demonstrated by a recent report in which heteroepitaxial Ta-doped SnO_2 (TTO) films exhibited low resistivity (1.1×10^{-4} Ω cm).[8]

A thermal design is important for optoelectronic devices composed of distinct films, such as organic light-emitting diodes (OLEDs) and solar cells because the luminescence and power-generation efficiencies, respectively, decrease with increasing temperature.[9–11] An effective thermal design thus requires highly accurate data on the thermophysical properties of the device's constituent layers, and some such data are available. For example, the thermal diffusivities of Sn-doped In_2O_3 (ITO) and In_2O_3–ZnO (IZO) films, both widely used as TCO films, have been reported. For 200-nm-thick ITO and IZO films, the thermal diffusivities are $(1.5–2.3) \times 10^{-6}$ and $(0.63–1.4) \times 10^{-6}$ m^2 s^{-1}, respectively, and are proportional to the electrical conductivities.[12,13] However, comparable data for ATO and TTO thin films, both of which are key materials for optoelectronic applications, have not yet been reported. Generally speaking, thermal energy in materials is transported mainly by free electrons and phonons. Thermal conduction via phonons should be strongly influenced by material components, dopant species, and material structure. We undertook a detailed analysis of the thermophysical properties of ATO and TTO thin films, including the effect of dopants (Sb and Ta) and material structure. Furthermore, we compare the results with analogous data of In_2O_3-, ZnO-, and TiO_2-based TCO films.

II. EXPERIMENT

We deposited 200-nm-thick ATO and TTO films with various electrical properties by rf magnetron sputtering from ceramic ATO and TTO targets, which lead to stable and highly reproducible deposition.[1–4] We measured the thermal diffusivity of the deposited films using the pulsed light heating thermoreflectance method with nanosecond laser pulses.[14–16]

Monolayer ATO and TTO films and trilayer Mo/(ATO or TTO)/Mo films were prepared by rf magnetron

Address all correspondence to these authors.
[a)]e-mail: n.oka@tagen.tohoku.ac.jp
[b)]e-mail: yuzo@chem.aoyama.ac.jp
[c)]Present affiliation: Institute of Multidisciplinary Research for Advanced Materials, Tohoku University, 2-1-1 Katahira, Aoba, Sendai 980-8577, Japan. e-mail: n.oka@tagen.tohoku.ac.jp.
This paper has been selected as an Invited Feature Paper.
DOI: 10.1557/jmr.2014.191

sputtering from high-density ceramic targets of SnO_2–Sb_2O_5 [Sb/(Sn + Sb) = 4 at.%] or SnO_2–Ta_2O_5 [Ta/(Sn + Ta) = 4 at.%] and Mo (99.95%, Furuuchi Chemical Corp.) onto fused silica substrates heated to 300 °C. For comparison, an amorphous ATO film was prepared by rf sputtering onto the unheated substrate. The ATO and TTO films were both 200 nm thick; the Mo films were 100 nm thick. The monolayer films were used to obtain the structural, electrical, and optical properties. The trilayer films were used to analyze the thermal diffusivity[17–24]; in these measurements, the top and bottom Mo layers were required to measure the thermoreflectance, which will be described later. The deposition chamber was evacuated to a pressure of $<7.0 \times 10^{-4}$ Pa. The rf power was 50 W. During ATO and TTO depositions, the total gas pressure P_{tot} was maintained at 1.0 Pa for sputtering gas (Ar) and reactive gas (O_2 or H_2). During Mo deposition, P_{tot} was maintained at 1.0 Pa for 100% Ar. A distance between the target and the substrate was 55 mm, and magnetic field strength was 0.1 T. The trilayer Mo/(ATO or TTO)/Mo structure was fabricated without atmospheric exposure between depositions.

The film thickness was estimated from the deposition rate and time, where the rate was calibrated by a surface profiler (Dektak3, Sloan Tech., Santa Barbara, CA). The electrical resistivity, Hall mobility, and carrier density of the films were determined by the four-point probe method and Hall effect measurements in the van der Pauw geometry (HL-5500PC, Bio-Rad, Hercules, CA). X-ray diffraction (XRD) measurements were conducted with Cu $K_{\alpha 1}$ radiation (XRD-6000, 40-kV, 20-mA, Shimadzu, Kyoto, Japan). Sb and Ta concentrations were measured by an electron probe microanalysis (JXA-8200, JEOL, Tokyo, Japan). The film transmittance and reflectance were measured from 190 to 2500 nm using a spectrophotometer (UV-3100, Shimadzu).

III. RESULTS

A. Structure

The XRD peaks from the (110), (101), (200), and (211) planes indicate that all ATO and TTO films deposited on heated substrates at 300 °C have a rutile SnO_2 polycrystalline structure. The concentrations of Sb [Sb/(Sn + Sb)] and Ta [Ta/(Sn + Ta)] in the ATO and TTO films are approximately 2.7 and 6.2 at.%, respectively.

B. Electrical and optical properties

Figure 1 shows the electrical resistivity ρ, Hall mobility μ, and carrier density n of the polycrystalline ATO and TTO films as a function of the reactive gas flow ratio (GFR) during deposition [given by either $O_2/(Ar + O_2)$ or $H_2/(Ar + H_2)$]. The carrier density is known to be dominated by oxygen vacancies and substitutional Sb^{5+} or Ta^{5+} ions at Sn^{4+} sites. The observed decrease in carrier density with increasing O_2 GFR is attributed to the extinction of O vacancies by enhanced oxidation. The lowest resistivities measured for the ATO and TTO films were 2.1×10^{-3} and 2.7×10^{-3} Ω cm, respectively, which compare favorably with those reported for ATO[1–7] and TTO[25] deposited by magnetron sputtering. In this study, we investigated the thermal diffusivity of films under conditions near those that provided the lowest resistivity. In the visible range, the transmittance of polycrystalline ATO and TTO films deposited near the conditions of lowest resistivity was around 80%, as shown in Fig. 2; in the near-infrared region, it decreased with increasing n whereas the

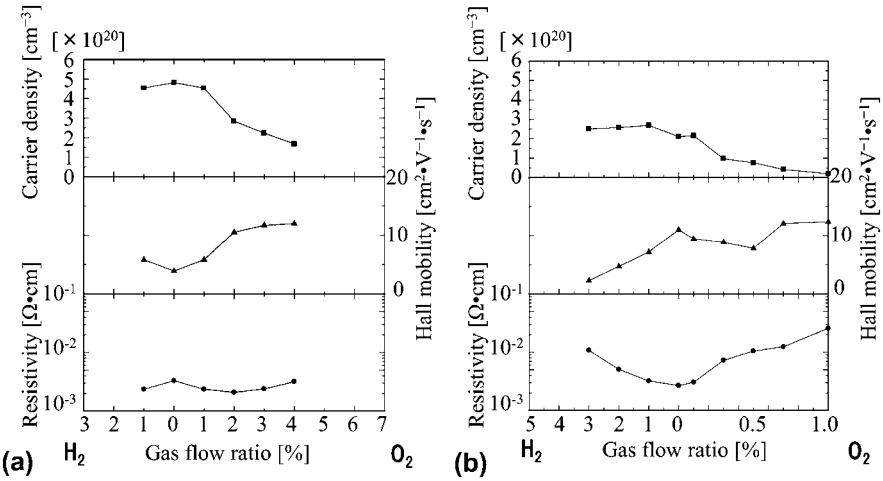

FIG. 1. Electrical resistivity, Hall mobility, and carrier density as a function of GFR [given either by $O_2/(Ar + O_2)$ or $H_2/(Ar + H_2)$] during film deposition for polycrystalline (a) ATO film and (b) TTO film.

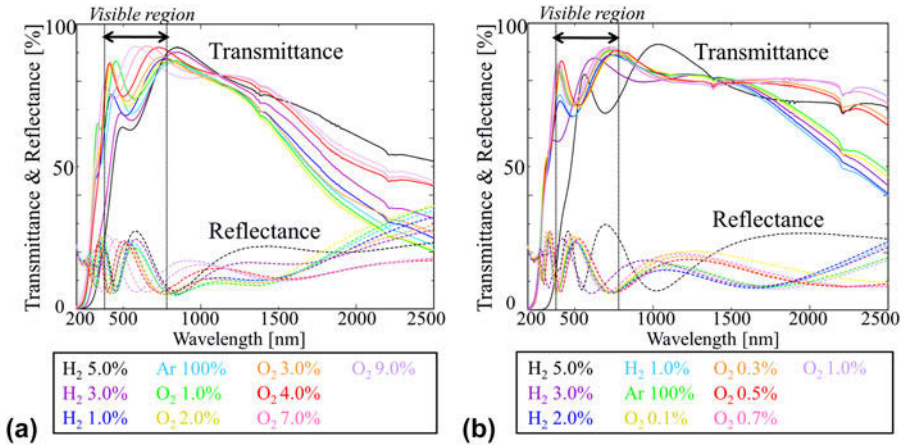

FIG. 2. Transmittance and reflectance spectra of (a) ATO film and (b) TTO film for several O_2 or H_2 GFRs [given either by $O_2/(Ar + O_2)$ or by $H_2/(Ar + H_2)$].

reflectance increased. These variations can be explained by Drude's theory.[26,27]

C. Thermophysical properties

Figure 3 shows a schematic of our pulsed light heating thermoreflectance system for measuring the thermal diffusivity. Figure 4 shows typical thermoreflectance results for the trilayer Mo/(ATO or TTO)/Mo films, where the inner polycrystalline ATO or TTO layers were deposited at the O_2 GFRs as shown in Figs. 1 and 2. We irradiated the bottom Mo layer (i.e., the Mo/substrate interface) with a 1064 nm pump laser to generate one-dimensional heat flow across the layered sample. Next, the temperature at the surface of the top Mo layer was detected by a 782 nm probe laser. The reflected probe beam was detected by a silicon photodiode. Because the thermoreflectance signal can be assumed to be proportional to temperature,[28] the signal rise time corresponds to the thermal diffusivity of the films. We analyzed the thermal diffusivities of the ATO and TTO films using a previously reported one-dimensional heat-flow model for trilayer films.[14,16,22] The film thickness d_{Mo} of the Mo layer was 100 nm, the thermal diffusivity κ_{Mo} was 1.7×10^{-5} m^2 s^{-1}, and the heat capacity C_{Mo} per unit volume was 2.53×10^6 J m^{-3} K^{-1}.[29] The ATO and TTO parameters were determined based on a heat capacity for SnO_2 of 53.2 J mol^{-1} K^{-1} (Ref. 23) and a density for SnO_2 of 6950 kg m^{-3},[24] which gives a heat capacity per unit volume of 2.45×10^6 J m^{-3} K^{-1}. We neglected the thermal boundary resistance between the outer Mo layer and the sandwiched inner layer because it should be considerably smaller than the total thermal resistance.[16,17,21,23] Our measurements indicate that the thermal diffusivity of the polycrystalline ATO and TTO films is $(1.8–2.0) \times 10^{-6}$ and 1.9×10^{-6} m^2 s^{-1}, respectively. The different dopants (Sb and Ta) do not appear to significantly influence the thermal diffusivity.

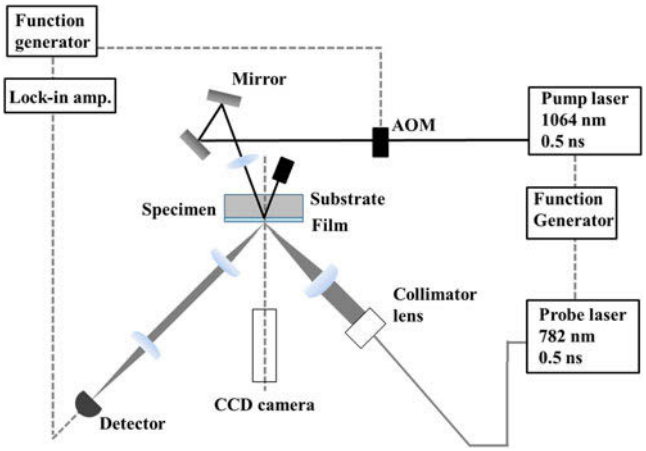

FIG. 3. Schematic of the pulsed light heating thermoreflectance system.

IV. DISCUSSION

Figure 5 shows the thermal conductivity λ plotted as a function of electrical conductivity σ for polycrystalline ATO and TTO films and for the amorphous ATO film, where λ is derived from the measured thermal diffusivity and from the specific heat capacity[30] and density[31] of SnO_2. For comparison, λ is also plotted for polycrystalline ITO films and amorphous ITO and IZO films.[12] At equivalent σ, λ for polycrystalline ATO and TTO films is higher than that of the ITO and IZO films. The TCO films are highly degenerate: free electrons behave similar to those in a metal. Thus, both free electrons and phonons should contribute to heat transport. The thermal conductivity λ_{el} carried by free electrons can be described by the Wiedemann–Franz law $\lambda_{el} = LT\sigma$, where L is the Lorentz number (2.45×10^{-8} W Ω K^{-2}) and T is absolute temperature. The dashed line in Fig. 5 gives the result for λ_{el} calculated from the Wiedemann–Franz law. The thermal conductivity λ_{ph} carried by phonons can be

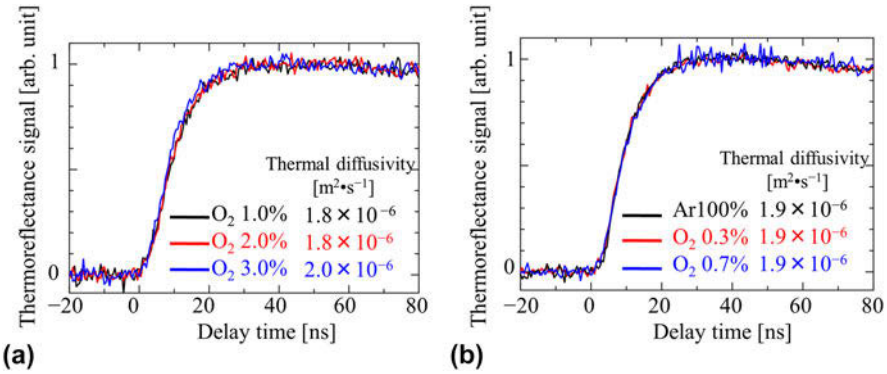

FIG. 4. Temporal thermoreflectance of trilayer Mo/(ATO or TTO)/Mo films. Inner layer is (a) ATO and (b) TTO.

estimated by subtracting λ_{el} from the measured total thermal conductivity: λ_{ph} differs significantly between polycrystalline and amorphous films, possibly because phonon corresponds to an atomic vibrational motion and its propagation is affected by crystallization. For polycrystalline ATO and TTO films, λ_{ph} is greater than that for polycrystalline ITO films. In general, λ_{ph} for metal oxides increases with approaching unity for the atomic mass ratio of "metal and oxygen," with a smaller unit cell, or with a simpler lattice structure (because of lattice vibrations or phonons).[18,19,32] Table I lists the metal/oxygen atomic mass ratio and the lattice structure for a base oxide material for various polycrystalline TCO films [i.e., ATO, TTO, ITO, Al-doped ZnO (AZO), and Nb-doped TiO_2 (NTO)]. Table II summarizes the thermophysical and electrical properties of these TCOs and amorphous IZO. The atomic mass ratios of Sn/O and In/O are almost the same. SnO_2 with a rutile structure has a considerably smaller unit cell and a simpler lattice structure than the bixbyite structure of In_2O_3, which may contribute significantly to higher λ_{ph} for ATO and TTO films. The same scheme can be applied to λ_{ph} of the other TCO materials, as shown in Table II.

In contrast, the dopant species (Sb or Ta) has a considerably smaller effect on λ_{ph} than does the base-material species (SnO_2 or In_2O_3). Although λ_{ph} in ITO is almost constant irrespective of dopant concentration,[12] λ_{ph} in NTO was reported to decrease with increasing dopant concentration.[19] The atomic weight ratio of Nb/Ti (1.94) is considerably greater than that of Sn/In (1.03), which should lead to more extensive phonon scattering in NTO than in ITO.[19] For ATO and TTO, the atomic mass ratios are Sb/Sn = 1.03 and Ta/Sn = 1.52, respectively. Currently, we cannot determine why λ_{ph} is only slightly affected by dopant species (Sb or Ta). One hypothesis is that, for transparent conductive SnO_2 films, the dopant concentration of Sb or Ta may be insufficient to significantly influence λ_{ph}.

Finally, λ of undoped SnO_2 single crystals was previously reported as 98 W m^{-1} K^{-1},[36] approximately 20 times higher than ATO and TTO films. Lower λ of these films can be attributed to the polycrystalline structure, and to structural defects generated by the dopants or the high energy particles, such as O^- bombarding on the growing film surface during sputter deposition.[37–40]

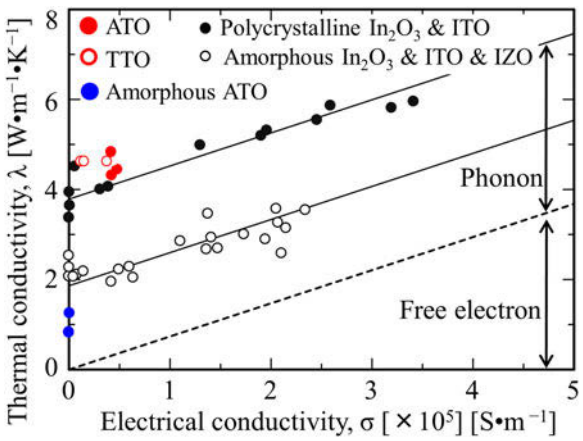

FIG. 5. Thermal conductivity as a function of electrical conductivity for ATO film (solid red circles) and TTO film (open red circles). Dotted line shows thermal conductivity calculated by the Wiedemann–Franz law. For comparison, the thermal conductivity of a polycrystalline ITO film (solid black circles) and an amorphous ITO and IZO film (open black circles)[12] is also plotted.

TABLE I. Atomic mass ratio of metal and oxygen, and lattice structure for SnO_2-, In_2O_3-, ZnO-, and TiO_2-based TCO films.

	Base oxide material	Atomic mass ratio (metal/oxygen)	Lattice structure
ATO, TTO	SnO_2	Sn/O = 7.4	Rutile structure containing 6 atoms per unit cell (Sn 2, O 4)
ITO	In_2O_3	In/O = 7.2	Bixbyite structure containing 80 atoms per unit cell (In 32, O 48)
AZO	ZnO	Zn/O = 4.1	Wurtzite structure containing 4 atoms per unit cell (Zn 2, O 2)
NTO	TiO_2	Ti/O = 3.0	Anatase structure containing 12 atoms per unit cell (Ti 4, O 8)

TABLE II. Thermophysical and electrical properties of SnO_2-, In_2O_3-, ZnO-, and TiO_2-based TCO films.

	Heat capacity per unit volume [$J \cdot m^{-3} \cdot K^{-1}$]	Thermal conductivity [$W \cdot m^{-1} \cdot K^{-1}$], Electrical conductivity [$S \cdot m^{-1}$]	Average λ_{ph} [$W \cdot m^{-1} \cdot K^{-1}$]
ATO	2.45×10^6 (SnO_2)[23, 24]	4.4–4.9, $(4.4–4.8) \times 10^4$	4.3
		[Amorphous] 0.8–1.3, below 3	1.0
TTO		4.7, $(1.0–3.7) \times 10^4$	4.5
ITO	2.58×10^6 (In_2O_3)[16]	4.0–6.0, $(0.3–3.4) \times 10^5$ (Ref. 12)	3.8
IZO (amorphous)		1.7–3.5, $(0–2.3) \times 10^5$ (Ref. 13)	1.7
AZO	2.83×10^6 (ZnO)[33, 34]	5.6–6.8, $(0.75–1.7) \times 10^5$ (Ref. 18)	5.4
NTO	2.77×10^6 (anatase TiO_2)[35]	5.7, below 3 (TiO_2 film)[19]	5.7
		4.0, below 3 [Nb/(Ti + Nb) = 3.2at%][19]	4.0
		3.3, below 3 [Nb/(Ti + Nb) = 8.5at%][19]	3.3
		4.2–4.6, $(1.6–1.9) \times 10^5$ [Nb/(Ti + Nb) = 8.5at%][19]	3.1

V. CONCLUSIONS

We measured the thermal diffusivity of 200-nm-thick ATO and TTO films by the pulsed light heating thermoreflectance method. ATO or TTO films sandwiched between 100-nm-thick Mo films [Mo/(ATO or TTO)/Mo] were fabricated by rf magnetron sputtering onto a fused silica substrate heated to 300 °C. During ATO and TTO film deposition, $Ar–O_2$ or $Ar–H_2$ gas mixtures were used to control the electrical conductivity of the films. The thermal diffusivities of the polycrystalline ATO and TTO films were measured to be $(1.8–2.0) \times 10^{-6}$ and 1.9×10^{-6} m^2 s^{-1}, respectively. The contribution of electrons to thermal transport is described by the Wiedemann–Franz law and that of phonons is almost constant, irrespective of the dopant species (Sb or Ta). Furthermore, the contribution of phonons to thermal transport is larger than that to polycrystalline ITO and amorphous ATO films. Compared with the effects of the base-material species and the structure (polycrystalline or amorphous), the dopant species has little effect on the thermophysical properties of transparent conductive ATO and TTO films. This knowledge allows us to form a strategy for choosing a material (base-material, dopant, structure) to optimize the thermal design for various industrial applications.

ACKNOWLEDGMENTS

This work was partially supported as a High-Tech Research Center project for private universities with matching funding from the Ministry of Education, Culture, Sports, Science and Technology (MEXT) of the Japanese Government.

REFERENCES

1. H.W. Lehmann and R. Widmer: Preparation and properties of reactively co-sputtered transparent conducting films. *Thin Solid Films* **27**(2), 359 (1975).
2. K. Suzuki and M. Mizuhashi: Structural, electrical and optical properties of r.f.-magnetron-sputtered SnO_2:Sb film. *Thin Solid Films* **97**(2), 119 (1982).
3. J. Ma, X. Hao, S. Huang, J. Huang, Y. Yang, and H. Ma: Comparison of the electrical and optical properties for SnO_2:Sb films deposited on polyimide and glass substrates. *Appl. Surf. Sci.* **214**, 208 (2003).
4. J. Lee: Effects of oxygen concentration on the properties of sputtered SnO_2:Sb films deposited at low temperature. *Thin Solid Films* **516**, 1386 (2008).
5. Y. Muto, N. Oka, N. Tsukamoto, Y. Iwabuchi, H. Kotsubo, and Y. Shigesato: High-rate deposition of Sb-doped SnO_2 films by reactive sputtering using the impedance control method. *Thin Solid Films* **520**, 1178 (2011).
6. B. Stjerna, E. Olsson, and C.G. Granqvist: Optical and electrical properties of radio frequency sputtered tin oxide films doped with oxygen vacancies, F, Sb, or Mo. *J. Appl. Phys.* **76**, 3797 (1994).
7. S. Jager, B. Szyszka, J. Szczyrbowski, and G. Brauer: Comparison of transparent conductive oxide thin films prepared by a.c. and d.c. reactive magnetron sputtering. *Surf. Coat. Technol.* **98**, 1304 (1998).
8. H. Toyosaki, M. Kawasaki, and Y. Tokura: Electrical properties of Ta-doped SnO_2 thin films epitaxially grown on TiO_2 substrate. *Appl. Phys. Lett.* **93**, 132109 (2008).
9. T. Sugiyama and Y. Furukawa: Noncontact temperature measurements of organic layers in an organic light-emitting diode using wavenumber–temperature relations of Raman bands. *Jpn. J. Appl. Phys.* **47**, 3537 (2008).
10. G. Vamvounis, H. Aziz, N-X. Hu, and Z.D. Popovic: Temperature dependence of operational stability of organic light emitting diodes based on mixed emitter layers. *Synth. Met.* **143**, 69 (2004).
11. G. Fraisse, C. Ménézo, and K. Johannes: Energy performance of water hybrid PV/T collectors applied to combisystems of direct solar floor type. *Sol. Energy* **81**, 1426 (2007).

12. T. Ashida, A. Miyamura, N. Oka, Y. Sato, T. Yagi, N. Taketoshi, T. Baba, and Y. Shigesato: Thermal transport properties of polycrystalline tin-doped indium oxide films. *J. Appl. Phys.* **105**, 073709 (2009).
13. T. Ashida, A. Miyamura, Y. Sato, T. Yagi, N. Taketoshi, T. Baba, and Y. Shigesato: Effect of electrical properties on thermal diffusivity of amorphous indium zinc oxide films. *J. Vac. Sci. Technol., A* **25**, 1178 (2007).
14. T. Baba: Analysis of one-dimensional heat diffusion after light pulse heating by the response function method. *Jpn. J. Appl. Phys.* **48**, 05EB04 (2009).
15. N. Taketoshi, T. Baba, and A. Ono: Electrical delay technique in the picosecond thermoreflectance method for thermophysical property measurements of thin films. *Rev. Sci. Instrum.* **76**, 094903 (2005).
16. T. Yagi, K. Tamano, Y. Sato, N. Taketoshi, T. Baba, and Y. Shigesato: Analysis on thermal properties of tin doped indium oxide films by picosecond thermoreflectance measurement. *J. Vac. Sci. Technol., A* **23**, 1180 (2005).
17. N. Oka, R. Arisawa, A. Miyamura, Y. Sato, T. Yagi, N. Taketoshi, T. Baba, and Y. Shigesato: Thermophysical properties of aluminum oxide and molybdenum layered films. *Thin Solid Films* **518**, 3119 (2010).
18. N. Oka, K. Kimura, T. Yagi, N. Taketoshi, T. Baba, and Y. Shigesato: Thermophysical and electrical properties of Al-doped ZnO films. *J. Appl. Phys.* **111**, 093701 (2012).
19. C. Tasaki, N. Oka, T. Yagi, N. Taketoshi, T. Baba, T. Kamiyama, S. Nakamura, and Y. Shigesato: Thermophysical properties of transparent conductive Nb-doped TiO_2 films. *Jpn. J. Appl. Phys.* **51**, 035802 (2012).
20. T. Yoshikawa, T. Yagi, N. Oka, J. Jia, Y. Yamashita, K. Hattori, Y. Seino, N. Taketoshi, T. Baba, and Y. Shigesato: Thermal conductivity of amorphous Indium–Gallium–Zinc oxide thin films. *Appl. Phys. Express* **6**, 021101 (2013).
21. S. Kawasaki, Y. Yamashita, N. Oka, T. Yagi, J. Jia, N. Taketoshi, T. Baba, and Y. Shigesato: Thermal boundary resistance of W/Al_2O_3 interface in $W/Al_2O_3/W$ three-layered thin film and its dependence on morphology. *Jpn. J. Appl. Phys.* **52**, 065802 (2013).
22. T. Yagi, N. Oka, T. Okabe, N. Taketoshi, T. Baba, and Y. Shigesato: Effect of oxygen impurities on thermal diffusivity of AlN thin films deposited by reactive RF magnetron sputtering. *Jpn. J. Appl. Phys.* **50**, 11RB01 (2011).
23. N. Oka, K. Kato, T. Yagi, N. Taketoshi, T. Baba, and Y. Shigesato: Thermal boundary resistance between N,N'-Di(1-naphthyl)-N,N'-diphenylbenzidine and aluminum films. *Jpn. J. Appl. Phys.* **50**, 11RB02 (2011).
24. N. Oka, K. Kato, T. Yagi, N. Taketoshi, T. Baba, N. Ito, and Y. Shigesato: Thermal diffusivities of tris(8-hydroxyquinoline) aluminum and N,N'-di(1-naphthyl)-N,N'-diphenylbenzidine thin films with sub-hundred nanometer thicknesses. *Jpn. J. Appl. Phys.* **49**, 121602 (2011).
25. Y. Muto, S. Nakatomi, N. Oka, Y. Iwabuchi, H. Kotsubo, and Y. Shigesato: High-rate deposition of Ta-doped SnO_2 films by reactive magnetron sputtering using a Sn–Ta metal-sintered target. *Thin Solid Films* **520**, 3746 (2012).
26. Y. Shigesato, D.C. Paine, and T.E. Haynes: Study of the effect of ion implantation on the electrical and microstructural properties of tin-doped indium oxide thin films. *J. Appl. Phys.* **73**, 3805 (1993).
27. I. Hamberg and C.G. Granqvist: Evaporated Sn-doped In_2O_3 films: Basic optical properties and applications to energy-efficient windows. *J. Appl. Phys.* **60**, R123 (1986).
28. N. Taketoshi, T. Baba, and A. Ono: Observation of heat diffusion across submicrometer metal thin films using a picosecond thermoreflectance technique. *Jpn. J. Appl. Phys.* **38**, L1268 (1999).
29. I. Barin and G. Platzki: In *Thermochemical Data of Pure Substances* (VCH, Weinheim, 1995).
30. I.S. Grigoriev and E.Z. Meilikhov: In *Handbook of Physical Quantities* (CRC Press, Boca Raton, 1997).
31. G.V. Samsonov.: In *The Oxide Handbook*, 2nd ed. (IFI/Plenum, New York, 1982).
32. T. Tsubota, M. Ohtaki, K. Eguchi, and H. Arai: Thermoelectric properties of Al-doped ZnO as a promising oxide material for high-temperature thermoelectric conversion. *J. Mater. Chem.* **7**, 85 (1997).
33. R.A. Robie, B.S. Hemingway, and J.R. Fisher: *Thermodynamic Properties of Minerals and Related Substances at 298.15 K and 1 bar (105 pascals) Pressure and at Higher Temperatures*, U.S. Geological Survey Bulletin (U.S. Govt. Printing Office, Washington D.C., 1978), Vol. **1452**, p. 248.
34. S-S. Lin, J-L. Huang, and D-F. Lii: The effects of r.f. power and substrate temperature on the properties of ZnO films. *Surf. Coat. Technol.* **176**, 173 (2004).
35. S.J. Smith, R. Stevens, S. Liu, G. Li, A. Navrotsky, J. Boerio-Goates, and B.F. Woodfield: Heat capacities and thermodynamic functions of TiO_2 anatase and rutile: Analysis of phase stability. *Am. Mineral.* **94**, 236 (2009).
36. P. Turkes, Ch. Pluntke, and R. Helbig: Thermal conductivity of SnO2 single crystals. *J. Phys. C: Solid State Phys.* **13** 4941 (1980).
37. N. Tsukamoto, D. Watanabe, M. Saito, Y. Sato, N. Oka, and Y. Shigesato: In situ analyses on negative ions in the sputtering process to deposit Al-doped ZnO films. *J. Vac. Sci. Technol., A* **28**, 846 (2010).
38. N. Ito, N. Oka, Y. Sato, and Y. Shigesato: Effects of energetic ion bombardment on structural and electrical properties of Al-doped ZnO films deposited by RF-superimposed DC magnetron sputtering. *Jpn. J. Appl. Phys.* **49**, 071103 (2010).
39. N. Tsukamoto, N. Oka, and Y. Shigesato: In-situ analyses on the reactive sputtering process to deposit Al-doped ZnO films using an Al–Zn alloy target. *Thin Solid Films* **520**, 3751 (2012).
40. N. Ito, S. Miyatake, N. Tsukamoto, N. Oka, Y. Sato, and Y. Shigesato: In-situ analyses on reactive sputtering processes to deposit photocatalytic TiO2 films. *Jpn. J. Appl. Phys.* **49**, 041105 (2010).